

Phase-resolved spectral analysis of 4U 1901+03 during its outburst

Ya-Juan Lei¹, Wei Chen¹, Jin-Lu Qu¹, Li-Ming Song¹, Shu Zhang¹, Yu Lu¹, Hao-Tong Zhang², Ti-Pei Li^{1,3}

¹*Particle Astrophysics Center, Institute of High Energy Physics, Chinese Academy of Sciences, Beijing 100049, P.R. China; leiyj@mail.ihep.ac.cn*

²*National Astronomical Observatories, Chinese Academy of Sciences, Beijing 100012, P.R. China*

³*Center for Astrophysics, Tsinghua University, Beijing 100084, P.R. China*

ABSTRACT

The high mass X-ray binary 4U 1901+03 was reported to have the pulse profile evolving with the X-ray luminosity and energy during its outburst in February–July 2003: the pulse peak changed from double to single along with the decreasing luminosity. We have carried out a detailed analysis on the contemporary phase-resolved energy spectrum of 4U 1901+03 as observed by Rossi X-ray Timing Explorer (*RXTE*). We find that, the spectra are phase dependent. At the begin of the outburst, the maximum of the optical depth for Compton scattering is near the major phase peak. During the decay of the outburst, the optical depth has the maximum being away from the main peak of the pulse profile. For each observation, Fe $K\alpha$ emission line is detected in the phase-resolved spectra, and its flux is constant across the pulse phases. This suggests an origin of Fe emission from the accretion disk but not the surface of the neutron star.

Subject headings: pulsars: individual (4U 1901+03)—stars: neutron—X-rays: stars

1. Introduction

Most of the known X-ray binary pulsars are the so-called high mass X-ray binary (HMXB). They are usually the Be/X-ray binaries characterized by the transient nature.

The Be star is an early-type nonsupergiant star with observable emission lines from the material in its circumstellar disk (see Slettebak 1988 for a review). Be/X-ray binaries usually show up with two types of outburst behavior: normal outburst with low X-ray luminosity lasting for days-weeks, and giant outbursts with higher X-ray luminosity ($L_X \gtrsim 10^{37}$ erg s $^{-1}$) occurring irregularly in every several years. Giant outbursts are thought to be driven by a dramatic expansion of the disk surrounding the Be star, which leads to the formation of an accretion disk around the compact object. Accompanying with the giant outburst, the neutron star is detected with the pulsed emission. The spectra of Be/X-ray binary are usually represented by a cutoff power law shape (e.g., Coburn et al. 2002; Corbet et al. 2009; Crawford et al. 2009). The iron K feature between 6 and 7 keV and low-energy absorption due to the cool material are as well observable (White et al. 1983; Wilson et al. 2008).

4U 1901+03 was detected as a Be/X-ray binary pulsar, one member of the HMXB (Liu et al. 2006). The orbital period and eccentricity of the system are measured as 22.58 d and 0.035, respectively. The period of X-ray pulsation is about 2.73 s (Galloway et al. 2005). The location of the source is R.A.=19^h04^m13^s.4 and Dec=+3°09′26″ (J2000.0) obtained by the observation with *Uhuru* (Forman et al. 1978; Friedhorsky & Terrell 1984). With the observation of *RXTE* Proportional Counter Array (PCA), Galloway et al. (2003a) obtained precise coordinates of R.A.=19^h03^m37^s.1, Dec=+3°11′31″.

There are two giant outbursts in the history of observations of 4U 1901+03. The first one was detected with *Uhuru* and Vela 5B in 1970-1971 (Forman et al. 1976; Friedhorsky & Terrell 1984). The second giant outburst took place in 2003 February, and was first detected by All Sky Monitor (ASM) on *RXTE*, followed by series of pointed *RXTE* observations over the next five months (Galloway et al. 2003b). At the hard X-rays, contemporary observations from INTEGRAL satellite are also available. During the second giant outburst, the X-ray flux of the source reached a value of $F_{2.5-25keV} \sim 8 \times 10^{-9}$ ergs cm $^{-2}$ s $^{-1}$.

Based on the *RXTE* observations, Galloway et al. (2005) made a thorough study on the orbital parameters, preliminary X-ray spectral analysis and pulse profiles from several observations for 4U 1901+03 during the 2003 giant outburst. Chen et al. (2008) carried out the detailed analysis of the energy dependence of the pulse profile along the outburst, and found that the pulse profile is correlated with both the X-ray luminosity and photon energy (Wang & Welter 1981; White et al. 1983; Nagase 1989; Mukerjee et al. 2000). The phase-resolved spectral analysis is need for studying the emission configure of Be/X-ray binary pulsar. Here we present for the first time phase-resolved spectra of 4U 1901+03 using all available *RXTE* data taken during the 2003 giant outburst. The paper is organized as the follows: description of observations and spectral model in Sec.2, results in Sect.3 and discussion finally in Sec.4.

2. Observation and data reduction

The observations analyzed in this paper are from PCA and High Energy X-Ray Timing Experiment (HEXTE) on board the *RXTE* satellite from February 10 to July 16 2003. The PCA consists of 5 non-imaging, coaligned Xe multiwire proportional counter units (PCUs) covering a nominal energy rang from 2 to 60 keV. Only PCU0 and PCU2 data are adopted in this work, which were on all the time during the observation of 4U 1901+03. The HEXTE instrument consists of two independent clusters (cluster A and cluster B) covering an energy range from 15 to 250 keV. Because detector 2 of cluster B of HEXTE lost its spectral capability and automatic gain control, only cluster A data are analyzed in the work. We extract light curves and spectra of PCA and HEXTE from intervals when the source has the offset angle of less than 0.02° and the limb of the earth is more than 10° with respect to the source direction. All HEXTE data products are dead-time corrected using the HEASOFT `ftool hxtdead`.

The data of Standard-2 and GoodXenon modes of the PCA and Archive and Science Event modes of the HEXTE are used to perform the spectra and timing analysis. The total lightcurve is extracted with Standard-2 mode data, and pulse-averaged X-ray spectra are extracted with Standard-2 and Science Event mode data. The pulse profiles of the chosen observations are extracted with GoodXenon, and the phase-resolved spectra are extracted with GoodXenon and Science Event data modes, using the software `fasebin`. Figure 1 shows the lightcurve of 2.0-21.0 keV, the soft and hard colors that are defined as the count rate ratios 4.5-6.1 keV/2.0-4.5 keV and 9.8-21.0 keV/6.1-9.8 keV, respectively.

The PCA background subtraction is carried out using the latest versions of the appropriate background models, and a 1 % systematic error is added to the spectra to account for the calibration uncertainties. Events in energy range ~ 2.5 -20 keV of the PCA and 17-80 keV of the HEXTE (17-50 keV for the late observations of the outburst) are selected for the spectral analysis with the software XSPEC version 12.3.0p (Arnaud 1996; Dorman & Arnaud 2001).

2.1. Spectral Model

According to the characteristic of the lightcurve (Fig. 1), we study the phase-averaged spectra of ten typical observations, carried out on February 10, 15, 22 and 23, March 27 and 30, April 30, May 25, June 14 and 28, respectively, , covering the outburst profile of the beginning, the peaking, the stepping down at the middle of decaying and the ending tail. Various spectral models are used to fit the phase-averaged spectra of these observations,

e.g., cutoffpl, powerlaw, bknpower, compTT, and a combination of each with a blackbody component. A gaussian component centered at 6-7 keV which represents fluorescent Fe line emission shows up as well in all spectra. A model consisting of compTT with a spherical geometry (Titarchuk 1994) and a Gaussian component is statistically acceptable ($\chi_{\text{red}}^2 \sim 1$) to fit the spectra (also see Galloway et al. 2005). Due to low effective area PCA below 3 keV, the column density n_{H} of neutral absorption can not be constrained well. Therefore, for all spectral fits we fix n_{H} at $1.2 \times 10^{22} \text{ cm}^{-2}$ (Galloway et al. 2005). Such a model can well fit the data till April 30. For the observations near the end of the outburst (May 25, June 14 and 28), an additional component of a blackbody has to be introduced in order to have a reasonable χ_{red}^2 . The temperature of the blackbody is $kT_{\text{bb}} \sim 1 \text{ keV}$. As an example, Figure 2 shows the fitting results with various models to the data of April 30.

We choose three typical observations on February 10, March 27, and April 30 to analyze the evolvement of the phase-resolved spectra. The phase-resolved spectra are extracted with eight phase bins. Figure 3 shows the spectra from the data of April 30, for phase bin No.5 (0.4375-0.5625). The fitting results of the spectra show the gaussian component is needed in the spectrum.

3. Results

3.1. Variation of soft and hard colors

Figure 1 shows a stepping down feature of the light curve, happened at time around April 30, during the decay of the outburst. The diagnosis on the pulse profile revealed a change from double peaks to single peak at this time (Chen et al. 2008). Accompanying to this as well are modifications in the fit model of the spectrum (Galloway et al. 2005; Chen et al. 2008). Along the decay of the outburst, the hard and the soft colors have the different evolutions: the soft color evolves similar to the light curve, while the hard color shows the opposite and ends up with a rapid decrease. The soft color and the hard color suggest an overall trend that the spectrum softens at the begin, but hardens with the decay of the outburst, and turns to soft at the end.

3.2. Phase-averaged spectra

Table 1 shows the results of the fit models on ten typical observations described in Sect.2, i.e., the beginning, the peaking, near stepping down and near the ending. The results show the temperature of the seed photons (T_0) in the Comptonization model is about

1 keV, and decreases slightly during the decay of the outburst. The temperature of the hot electronic population (kT) remained at about 5 keV. The optical depths of the observations from February 10 to April 30 are consistent with a flat distribution within the error bars, and an average is derived as ~ 5 . At the end of the outburst, the optical depths are obtained as 7-8. We notice that, the Fe K α line emission with equal width ~ 100 eV presents at around 6.5 keV in the energy spectrum, and its flux varies between $\sim 1-10 \times 10^{-11}$ ergs cm $^{-2}$ s $^{-1}$, showing a trend of increasing with the intensity. At the end of outburst, an additional spectral component of a blackbody is needed for spectral fittings.

3.3. Phase-resolved spectra

For studying the evolution of the phase-resolved spectra, we choose the typical observations with the high signal-to-noise ratio, i.e., on February 10, March 27 and April 30. The spin lightcurve of each observation is subdivided into 8 phases, for each the energy spectrum is extracted, and the flux is shown in Figure 4. Figure 4 shows the phase dependence of the spectra of the three observations. The pulse profile of the three observations are best presented in Figure 4, each with 32 phase bins. At the beginning of the outburst (February 10), the optical depth maximizes near the major phase peak. However, during the decay of the outburst, such maximum moves towards the second one, and the temperature of the scattering electron has a trend of anti-correlation with the optical depth. The center energy of Fe line is almost around 6.5 keV. For each observation, the fluxes of iron line are likely constant across the whole pulse phases. The spectra from the phases (1 for February 10, 2 for March 27 and 2 for April 30) of the lowest intensity present as well the existence of the obvious Fe feature, as shown in Figure 5 is an example from the phase 2 of the data of April 30, with the fluxes comparable to those from what else phases (Fig. 4).

3.4. Spectral Ratios

The detailed phase-to-phase variation is best illustrated by ratios of the phase-resolved spectra to the spectrum of the phase with minimum count rate (Leahy & Matsuoka 1990). We show the phase-resolved spectral ratios of the three observations. The minimum-count-rate spectra are from phase 1 for observation of February 10, phase 2 for both observations of March 27 and April 30. The phase ratios are then presented separately in Figure. 6-8. There are dips in the PHA plots at ~ 6.5 keV (as marked by the arrow in the first panel of Fig. 6). The dip is due to that flux of Fe emission line that only occurs in non-pulse component, this is consistent with the results of the phase-resolved spectra.

For the phase 2 of February 10, at the beginning of the main pulse, the ratios increase with energy. The ratio increases with energies rapidly at the phase 3 where the main pulse is peaking, but slowly at the phases (4 and 5) beyond. As is the case as well for at the end of the main pulse (phase 6), till the energies around 10 keV, beyond which the ratio remains almost constant. Such a trend holds more or less in phases 7 and 8, corresponding to the second pulse, but with a turn over of the ratio at energies larger than 10 keV. For March 27, the properties of PHA ratios are similar to those for February 10. For April 30, phases 3, 4 and 5 correspond to the main pulse peak. The PHA ratios of these phases are increase with energy, but are constant at above 10 keV. Phases 6, 7, 8 and 1 are around the second pulse, and their PHA ratios increase at low energy (<10 keV), and decrease at 10-20 keV. The overall spectral ratio of April 30 is different from those of February 10 and March 27.

The PHA ratios of the phase-resolved to the phase with minimum count rate are increasing with energy, illuminating that the spectra of the pulsed are generally harder. The stronger the flux of the pulsed, the harder the spectrum. At the phases around the second pulse, the spectrum decreases abruptly at higher energies.

4. Discussion

The X-ray radiation modes of Be/X-ray binary pulsar is generally thought to have tight relation with the luminosity (Parmar et al. 1989). At high luminosity ($\gtrsim 10^{37}$ ergs s^{-1}), the accretion flow onto the magnetic pole can be decelerated via the radiative shock formed near the neutron star surface (Wang & Frank 1981). The emitting plasma will be compressed under the shocked region, where the photons can only escape from the sides of the column (fan-beam mode). Under some circumstances, a pencil-beam may still emerge (Nagel 1981). At lower luminosity ($\lesssim 10^{37}$ ergs s^{-1}) the infalling material may be decelerated in a collisionless shock above the neutron star surface (Basko & Sunyaev 1975; Kirk & Galloway 1981). In such a case, a thin emitting region or effects of the strong magnetic field can cause a pencil-beam of emission to be formed (e.g., Mészáros et al. 1983). The various models could be verified by the observational properties of X-ray pulsars.

We have analyzed the phase-resolved spectra of 4U 1901+03, and found that the optical depth and the temperature of the scattering electron are related to the pulse phases, which is a common feature of X-ray pulse binary (e.g., La Barbera et al. 2003). Spectral ratios indicate the main pulse peak has the hardest spectrum, which is common property of accreting pulsars (Hickox & Vrtilik 2005; Tsygankov et al. 2007). Our results show, at the beginning of the outburst (February 10) where the luminosity ($\gtrsim 10^{37}$ ergs s^{-1}), the emission of the main pulse has the possible origins of the fan-beam. The main pulse has the large

optical depth, could be due to that, during the main peak, the angle between the column axis and the observer’s line of sight has the highest value so that the observer is looking almost along the beam (Klochkov et al. 2008). During the decay of the outburst, our results are consistent with the emission configuration that the main peak from the fan-beam and the second peak from pencil-beam (Chen et al. 2008), the main peak that has the hard spectrum is due to that high energy photons are more liable to escape in a fan-beam from a hot region close to the footstep and perpendicular to the accretion column (Basko & Sunyaev 1976; White et al. 1983; Klochkov et al. 2008), which is consistent with the low optical depth and high temperature of the scattering electron of the main peak. The second peak is produced by the low energy photons escaping in a pencil-beam along the direction of the accretion column where the optical depth is larger and the electron temperature is lower. These results are accordant to those of Chen et al. (2008) who analyzed energy-resolved pulse profiles in details. They concluded as well that, the fan-beam contributes to the main pulse peak and pencil-beam to the second pulse peak. In addition, in some energy bands the flux varies by almost a factor of two between different pulse phases (Chen et al. 2008), both the angles of the spin-axis from the viewing direction and between the magnetic pole and the spin-axis are substantial. Therefore, it is likely that emission from both magnetic poles contribute to the pulse profile.

We notice that the evolution of hard color is similar to that of pulse fraction (see Chen et al. 2008), and spectral ratios show that the spectra of the pulsed are harder than those of the non-pulsed under larger pulsed fluxes. This indicates that the high energy photons contribute mostly to the pulsed emission, which is consistent with the evolvement of the pulse fraction shown by Figure 4 of Chen et al. (2008). Perhaps the lower energy radiation is dominated by photons from the accretion column walls that hit the neutron star surface and are reprocessed, which would lead to a lower pulse fraction.

Fe $K\alpha$ emission line with equivalent widths of several hundred eV is usually detected in X-ray pulsar, may be caused by illumination of neutral or partially ionized material in the accretion disk, stellar wind of the high-mass companion, or material in the line of sight or in the accretion column (Pravdo et al. 1977; Basko 1980; Nagase 1985; Paul et al. 2002; Naik et al. 2005). Our results show that prominent Fe emission with equivalent width ~ 100 eV is detected in the spectra of 4U 1901+03. The flux of Fe emission line is increasing with the X-ray luminosity along the outburst (Fig. 1 and Table 1), and is proportional to that of continuum intensity and increases with increasing of the accretion rate (Suchy et al. 2008). For each observation, Fe line is detected in the spectra of the continuum in each pulse phase and its flux is constant within errors, and is not correlated with pulse phases. Therefore, the Fe line of 4U 1901+03 is not likely to origin from the accretion column of magnetic polar cap. Furthermore, the spectral fit of the phase-resolved spectrum shows that, the center energy

of Fe neither change among the pulse phases nor evolve along the outburst of 4U 1901+03. We therefore believe that, during the outburst of 4U 1901+03, Fe emissions should come from a region in the accretion disk but not the surface of the neutron star.

Acknowledgments

The authors are grateful to the referee for the helpful comments. We are thankful for Prof. F.J. Lu for the useful discussions. This work is subsidized by the Special Funds for Major State Basic Research Projects and by the Natural Science Foundation of China for support via NSFC 10903005, 10773017, 10325313, 10521001, 10733010, Xinjiang Uygur Autonomous Region of China (Program 200821164) and program of the Light in Chinese Western Region (LCWR) under grant LHXZ 200802, the CAS key project via KJCX2-YWT03, and 973 Program 2009CB824800.

REFERENCES

- Arnaud, K. A. 1996, *Astronomical Data Analysis Software and Systems V*, 101, 17
- Basko, M. M. 1980, *A&A*, 87, 330
- Basko, M. M., & Sunyaev, R. A. 1975, *A&A*, 42, 311
- Basko, M. M., & Sunyaev, R. A. 1976, *MNRAS*, 175, 395
- Chen, W., Qu, J.-L., Zhang, S., Zhang, F., & Zhang, G.-B. 2008, *Chinese Astronomy and Astrophysics*, 32, 241
- Coburn, W., Heindl, W. A., Rothschild, R. E., Gruber, D. E., Kreykenbohm, I., Wilms, J., Kretschmar, P., & Staubert, R. 2002, *ApJ*, 580, 394
- Corbet, R. H. D., in't Zand, J. J. M., Levine, A. M., & Marshall, F. E. 2009, *ApJ*, 695, 30
- Crawford, F., Lorimer, D. R., Devour, B. M., Takacs, B. P., & Kondratiev, V. I. 2009, *ApJ*, 696, 574
- Dorman, B., & Arnaud, K. A. 2001, *Astronomical Data Analysis Software and Systems X*, 238, 415
- Forman, W., Jones, C., Cominsky, L., Julien, P., Murray, S., Peters, G., Tananbaum, H., & Giacconi, R. 1978, *ApJS*, 38, 357

- Forman, W., Tananbaum, H., & Jones, C. 1976, *ApJ*, 206, L29
- Galloway, D. K., Remillard, R., & Morgan, E. 2003a, *IAU Circ.*, 8081, 2
- Galloway, D., Remillard, R., Morgan, E., & Swank, J. 2003b, *IAU Circ.*, 8070, 2
- Galloway, D. K., Wang, Z., & Morgan, E. H. 2005, *ApJ*, 635, 1217
- Hickox, R. C., & Vrtilik, S. D. 2005, *ApJ*, 633, 1064
- Kirk, J. G., & Galloway, D. J. 1981, *MNRAS*, 195, 45P
- Klochkov, D., Santangelo, A., Staubert, R., & Ferrigno, C. 2008, *A&A*, 491, 833
- La Barbera, A., Santangelo, A., Orlandini, M., & Segreto, A. 2003, *A&A*, 400, 993
- Leahy, D. A., & Matsuoka, M. 1990, *ApJ*, 355, 627
- Liu, Q. Z., van Paradijs, J., & van den Heuvel, E. P. J. 2006, *A&A*, 455, 1165
- Meszaros, P., Harding, A. K., Kirk, J. G., & Galloway, D. J. 1983, *ApJ*, 266, L33
- Mukerjee, K., Agrawal, P. C., Paul, B., Rao, A. R., Seetha, S., & Kasturirangan, K. 2000, *A&A*, 353, 239
- Nagase, F. 1985, *Galactic and Extra-Galactic Compact X-ray Sources*, 7
- Nagase, F. 1989, *PASJ*, 41, 1
- Nagel, W. 1981, *ApJ*, 251, 288
- Naik, S., Callanan, P. J., & Paul, B. 2005, *Interacting Binaries: Accretion, Evolution, and Outcomes*, 797, 593
- Parmar, A. N., White, N. E., & Stella, L. 1989, *ApJ*, 338, 373
- Paul, B., Dewangan, G. C., Sako, M., Kahn, S. M., Paerels, F., Liedahl, D., Wojdowski, P., & Nagase, F. 2002, *8th Asian-Pacific Regional Meeting, Volume II*, 355
- Pravdo, S. H., Becker, R. H., Boldt, E. A., Holt, S. S., Serlemitsos, P. J., & Swank, J. H. 1977, *ApJ*, 215, L61
- Priedhorsky, W. C., & Terrell, J. 1984, *ApJ*, 280, 661
- Slettebak, A. 1988, *PASP*, 100, 770

Suchy, S., et al. 2008, ApJ, 675, 1487

Titarchuk, L. 1994, ApJ, 434, 570

Tsygankov, S. S., Lutovinov, A. A., Churazov, E. M., & Sunyaev, R. A. 2007, Astronomy Letters, 33, 368

Wang, Y.-M., & Frank, J. 1981, A&A, 93, 255

Wang, Y.-M., & Welter, G. L. 1981, A&A, 102, 97

White, N. E., Swank, J. H., & Holt, S. S. 1983, ApJ, 270, 711

Wilson, C. A., Finger, M. H., & Camero-Arranz, A. 2008, ApJ, 678, 1263

Table 1: **Fit parameters for the spectra.**

| date | T_0 (keV) | kT (keV) | τ | E_{Fe} (keV) | Flux _{Fe} | χ^2_{red} | | |
|--------|---------------------------|------------------------|------------------------|--------------------------|-------------------------|---------------------------|--------------------|-----------------------|
| Feb.10 | $1.027^{+0.026}_{-0.072}$ | $5.28^{+0.15}_{-0.27}$ | $4.95^{+0.45}_{-0.15}$ | $6.45^{+0.13}_{-0.58}$ | $6.35^{+14.13}_{-1.88}$ | 1.14 | | |
| Feb.15 | $1.117^{+0.019}_{-0.021}$ | $5.09^{+0.06}_{-0.07}$ | $4.96^{+0.09}_{-0.09}$ | $6.52^{+0.12}_{-0.12}$ | $7.85^{+2.46}_{-1.85}$ | 0.91 | | |
| Feb.22 | $1.128^{+0.023}_{-0.027}$ | $4.87^{+0.11}_{-0.09}$ | $5.01^{+0.15}_{-0.14}$ | $6.54^{+0.11}_{-0.12}$ | $8.98^{+3.04}_{-2.20}$ | 0.92 | | |
| Feb.23 | $1.114^{+0.025}_{-0.030}$ | $4.86^{+0.14}_{-0.09}$ | $4.98^{+0.17}_{-0.15}$ | $6.53^{+0.11}_{-0.11}$ | $9.85^{+3.65}_{-2.40}$ | 0.74 | | |
| Mar.27 | $1.028^{+0.038}_{-0.063}$ | $4.70^{+0.21}_{-0.21}$ | $4.98^{+0.37}_{-0.25}$ | $6.54^{+0.14}_{-0.20}$ | $9.13^{+7.46}_{-3.01}$ | 0.65 | | |
| Mar.30 | $0.991^{+0.029}_{-0.046}$ | $4.70^{+0.12}_{-0.13}$ | $5.09^{+0.24}_{-0.17}$ | $6.46^{+0.12}_{-0.17}$ | $8.87^{+5.54}_{-2.49}$ | 0.92 | | |
| Apr.30 | $0.898^{+0.036}_{-0.049}$ | $4.90^{+0.21}_{-0.19}$ | $5.15^{+0.26}_{-0.22}$ | $6.41^{+0.12}_{-0.16}$ | $5.27^{+3.04}_{-1.57}$ | 0.98 | | |
| date | T_0 (keV) | kT (keV) | τ | E_{Fe} (keV) | Flux _{Fe} | kT_{bb} (keV) | $norm_{\text{bb}}$ | χ^2_{red} |
| May.25 | $0.80^{+0.11}_{-0.21}$ | $4.61^{+0.23}_{-0.23}$ | $7.38^{+0.92}_{-0.97}$ | $6.48^{+0.12}_{-0.16}$ | $1.53^{+0.61}_{-0.41}$ | $1.15^{+0.08}_{-0.17}$ | 31^{+37}_{-6} | 0.56 |
| Jun.14 | $1.00(\text{fixed})$ | $4.75^{+0.32}_{-0.32}$ | $7.23^{+1.32}_{-0.85}$ | $6.67^{+0.14}_{-0.15}$ | $1.31^{+0.58}_{-0.41}$ | $0.92^{+0.06}_{-0.05}$ | 52^{+9}_{-7} | 0.71 |
| Jun.28 | $0.52^{+1.03}_{-0.52}$ | $5.01^{+0.40}_{-0.33}$ | $7.67^{+1.30}_{-0.98}$ | $6.59^{+0.20}_{-0.18}$ | $0.54^{+0.53}_{-0.22}$ | $0.91^{+0.06}_{-0.13}$ | 25^{+16}_{-6} | 0.80 |

Note. — T_0 is the temperature of the soft seed photons for the Comptonization, kT is the electron temperature, τ is the optical depth of the scattering cloud in a spherical geometry. E_{Fe} is the central energy of Gaussian emission line, and Flux_{Fe} is the flux of Gaussian emission line in units of 10^{-11} ergs cm⁻² s⁻¹. kT_{bb} is the temperature of blackbody, and $norm_{\text{bb}}$ is the normalization of blackbody.

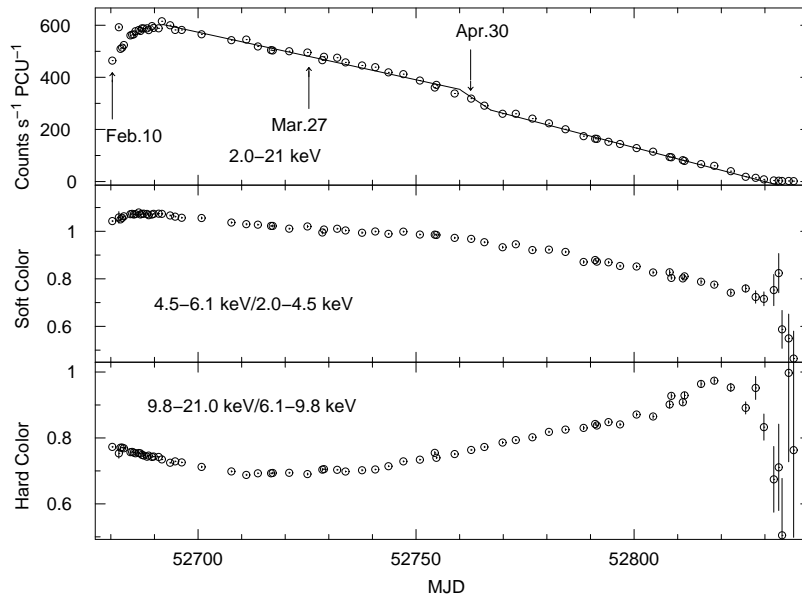


Fig. 1.— From top to bottom: the total light curve, the soft color, and the hard color, respectively.

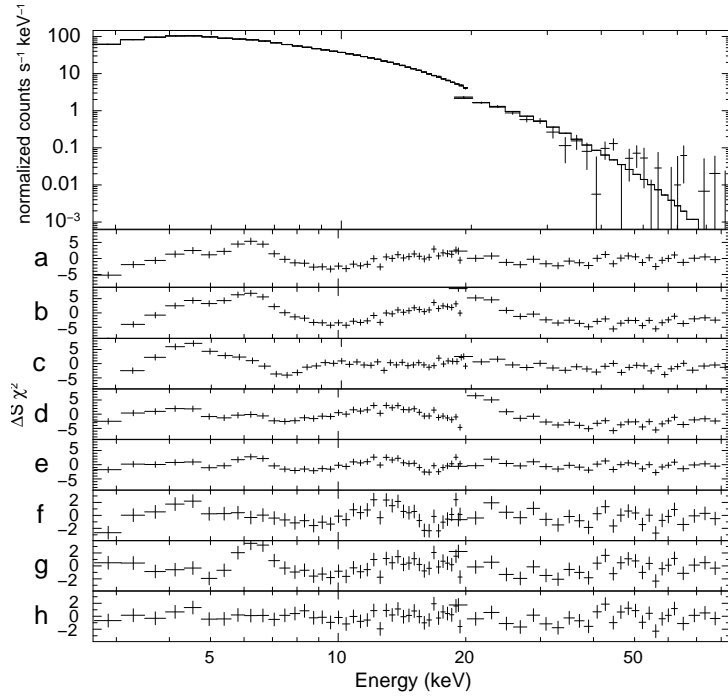


Fig. 2.— PCA spectrum for the observation of April 30 and the best-fit model. The residuals are shown sequentially taking (a) the cutoffpl model ($\chi_{\text{red}}^2=3.96$), (b) the powerlaw+bbbody model ($\chi_{\text{red}}^2=13.15$), (c) the powerlaw+bbbody+gaussian ($\chi_{\text{red}}^2=6.38$), (d) the bknpower model ($\chi_{\text{red}}^2=9.04$), (e) the bknpower+bbbody model ($\chi_{\text{red}}^2=2.09$), (f) the bknpower+bbbody+gaussian ($\chi_{\text{red}}^2=1.75$), (g) the compTT model ($\chi_{\text{red}}^2=1.69$), (h) the compTT+gaussian model ($\chi_{\text{red}}^2=0.98$).

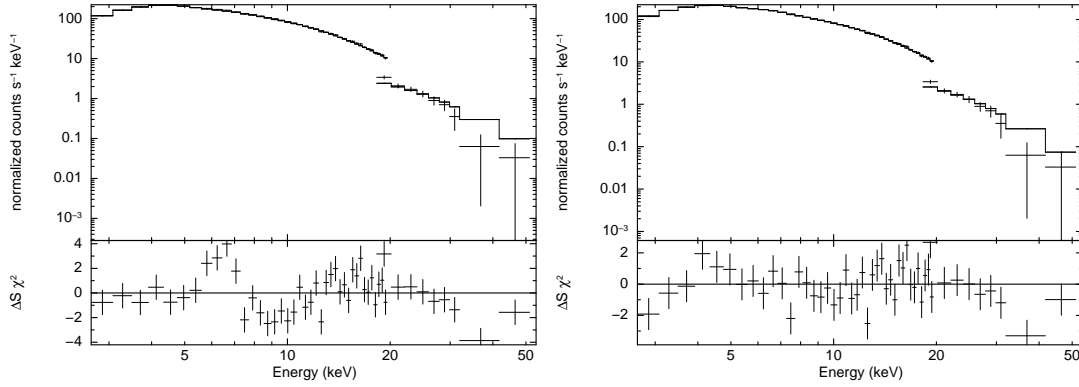


Fig. 3.— The fitting results of the phase-resolved spectrum of the phase 5 of the observation April 30, the left panel shows the fitting result by the model without Gaussian component, the residual shows obvious Fe line profile; the right panel shows the fitting result with the model containing the Gaussian component, the residual is removed.

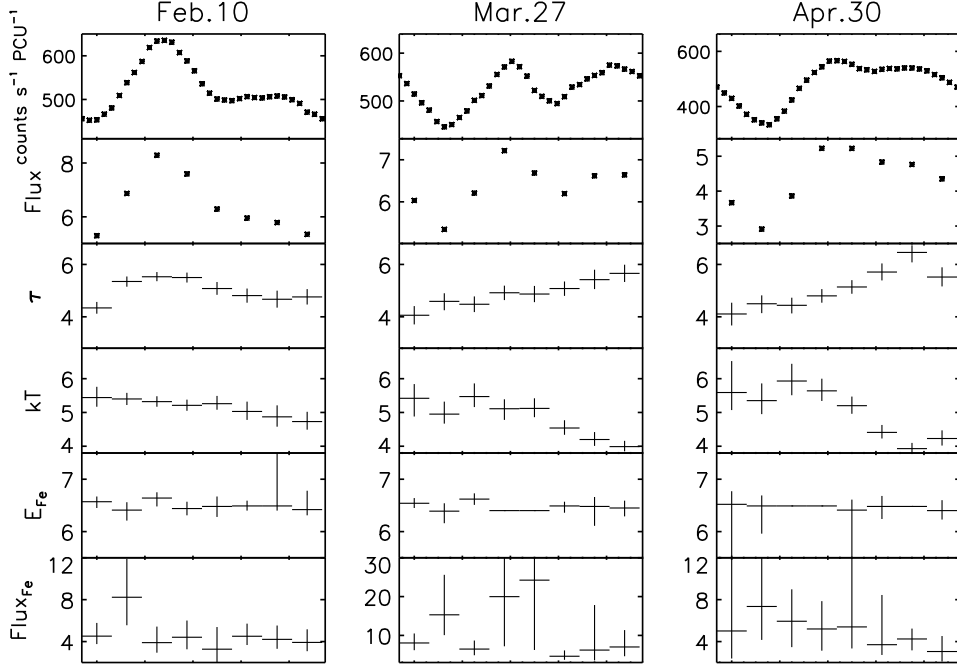


Fig. 4.— The phase-resolved spectral parameters as a function of pulse phases. From top to bottom: the pulse profiles of 32 phase bins obtained from all PCA channels (2-60 keV), the flux of 3-30 keV of 8 phase bins in units of 10^{-9} ergs cm^{-2} s^{-1} , optical depth for Compton scattering, the temperature of the scattering electron cloud, the central energy and flux of Fe emission line. The central energies of Fe line are fixed for phases 4 and 5 of March 27 and phases 3 and 4 of April 30.

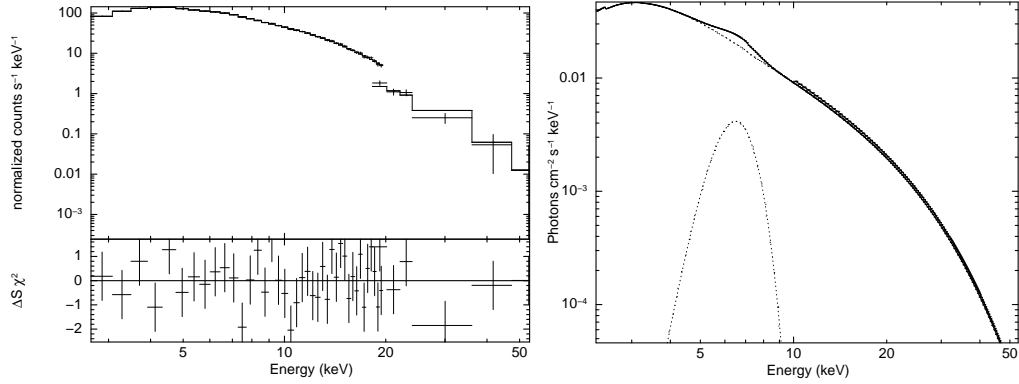


Fig. 5.— The fitting result of the spectrum of the phase 2 of the observation April 30. The left panel shows the fitting result and residual, the right panel shows the model components of (compTT+gaus).

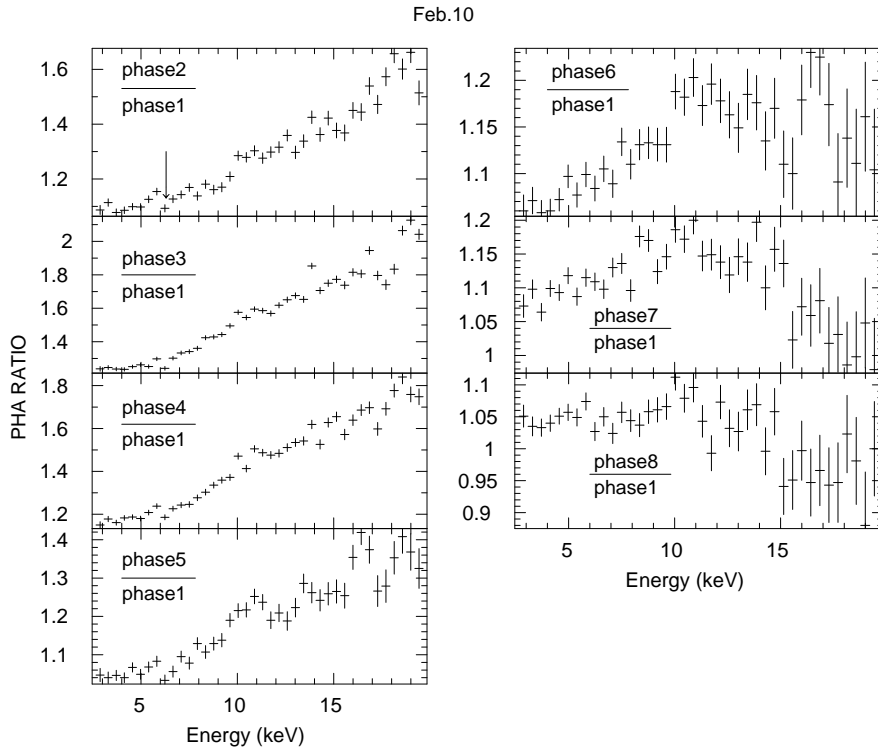


Fig. 6.— Ratios of intensity in narrow energy bands from February 10 phase 2-8 spectra to intensity from phase 1 spectrum.

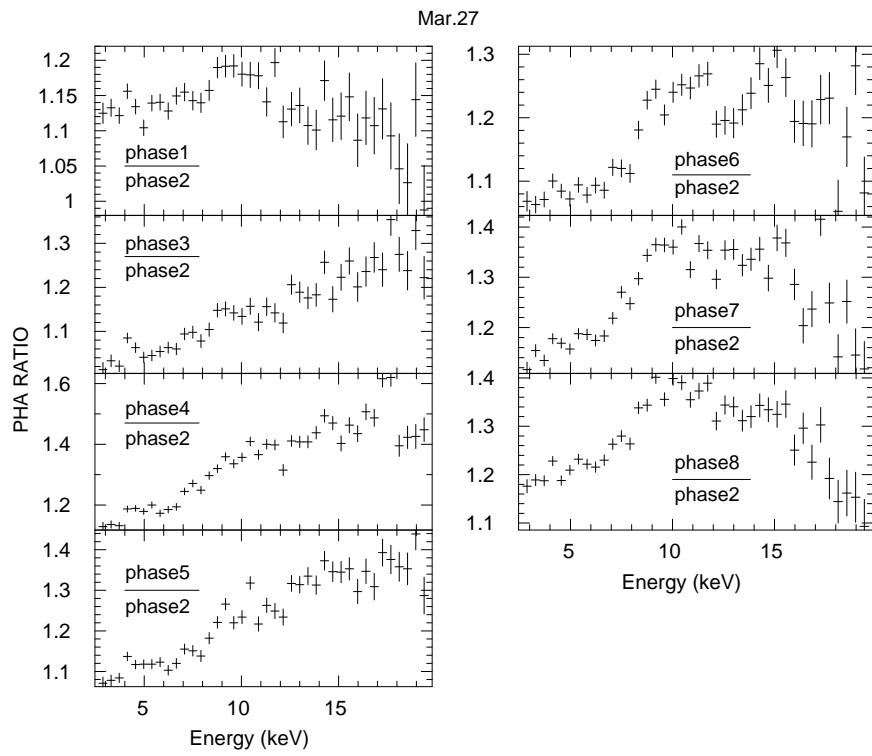


Fig. 7.— Similar to Figure 6, but for March 27.

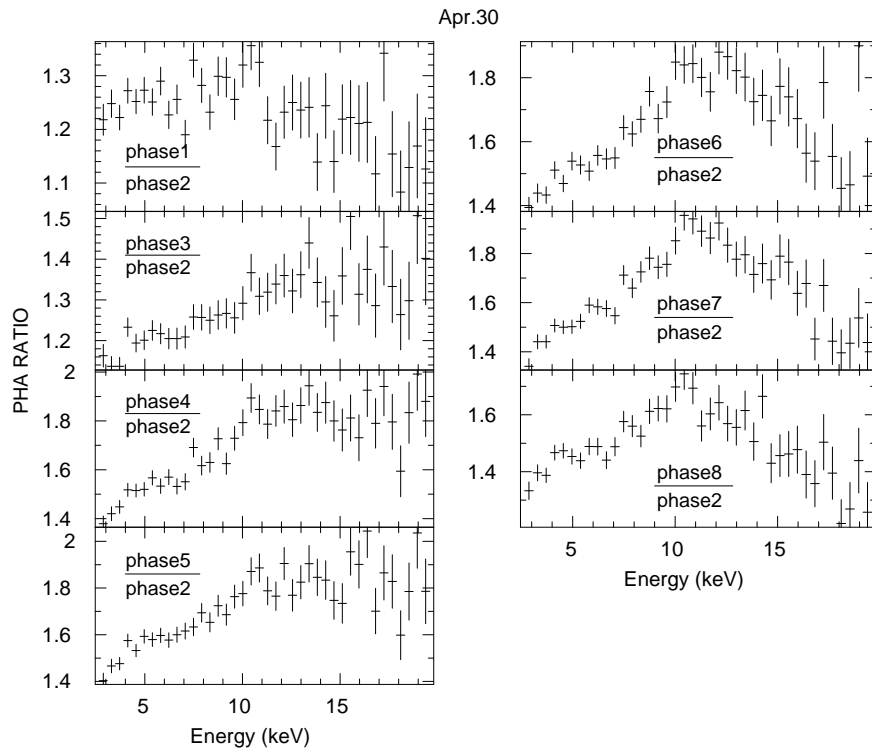


Fig. 8.— Similar to Figure 6, but for April 30.